

#### **OPEN ACCESS**

# Transient Self-Discharge after Formation in Lithium-Ion Cells: Impact of State-of-Charge and Anode Overhang

To cite this article: Thomas Roth et al 2023 J. Electrochem. Soc. 170 080524

View the article online for updates and enhancements.

### You may also like

- <u>Modeling Voltage Decay During Calendar-Life Aging</u>
   Dongliang Lu, M. Scott Trimboli, Yujun Wang et al.
- Revisiting the t<sup>0.5</sup> Dependence of SEI Growth
   Peter M. Attia, William C. Chueh and Stephen J. Harris
- A Comparison of Voltage Hold and Voltage Decay Methods for Side Reactions Characterization Luiza Streck, Thomas Roth, Peter Keil et



## Your Lab in a Box!

The PAT-Tester-i-16: All you need for Battery Material Testing.

- ✓ All-in-One Solution with integrated Temperature Chamber!
- ✓ Cableless Connection for Battery Test Cells!
- ✓ Fully featured Multichannel Potentiostat / Galvanostat / EIS!

www.el-cell.com +49 40 79012-734 sales@el-cell.com









# Transient Self-Discharge after Formation in Lithium-Ion Cells: Impact of State-of-Charge and Anode Overhang

Thomas Roth, <sup>1,z</sup> Luiza Streck, <sup>1</sup> Nedim Mujanovic, <sup>1</sup> Martin Winter, <sup>2</sup> Philip Niehoff, <sup>2</sup> and Andreas Jossen <sup>1</sup>

<sup>1</sup>Technical University of Munich, School of Engineering and Design, Department of Energy and Process Engineering, Chair of Electrical Energy Storage Technology, 80333 Munich, Germany

A fast determination of cell quality after formation is challenging due to transient effects in the self-discharge measurement. This work investigated the self-discharge of NMC622/graphite single-layer pouch cells with varying anode dimensions to differentiate between SEI growth and anode overhang equalization processes. The transient self-discharge was measured directly after formation via voltage decay and for 20 weeks of calendar storage at three states-of-charge (SOC), 10%, 30%, and 50%. The transient behavior persisted for the entire measurement duration, even at a low SOC. Still, the low SOC minimized the impact of SEI growth and anode overhang equalization compared to moderate SOCs. Evaluating the coulombic efficiency from cycle aging showed a distinct capacity loss for the first cycle after storage, indicating further SEI growth, which stabilized in subsequent cycles. The aged capacity after cycling showed no significant dependence on the calendar storage, which further promotes fast self-discharge characterization at low SOC.

© 2023 The Author(s). Published on behalf of The Electrochemical Society by IOP Publishing Limited. This is an open access article distributed under the terms of the Creative Commons Attribution 4.0 License (CC BY, http://creativecommons.org/licenses/by/4.0/), which permits unrestricted reuse of the work in any medium, provided the original work is properly cited. [DOI: 10.1149/1945-7111/acf164]

Manuscript submitted June 23, 2023; revised manuscript received August 3, 2023. Published August 29, 2023.

Supplementary material for this article is available online

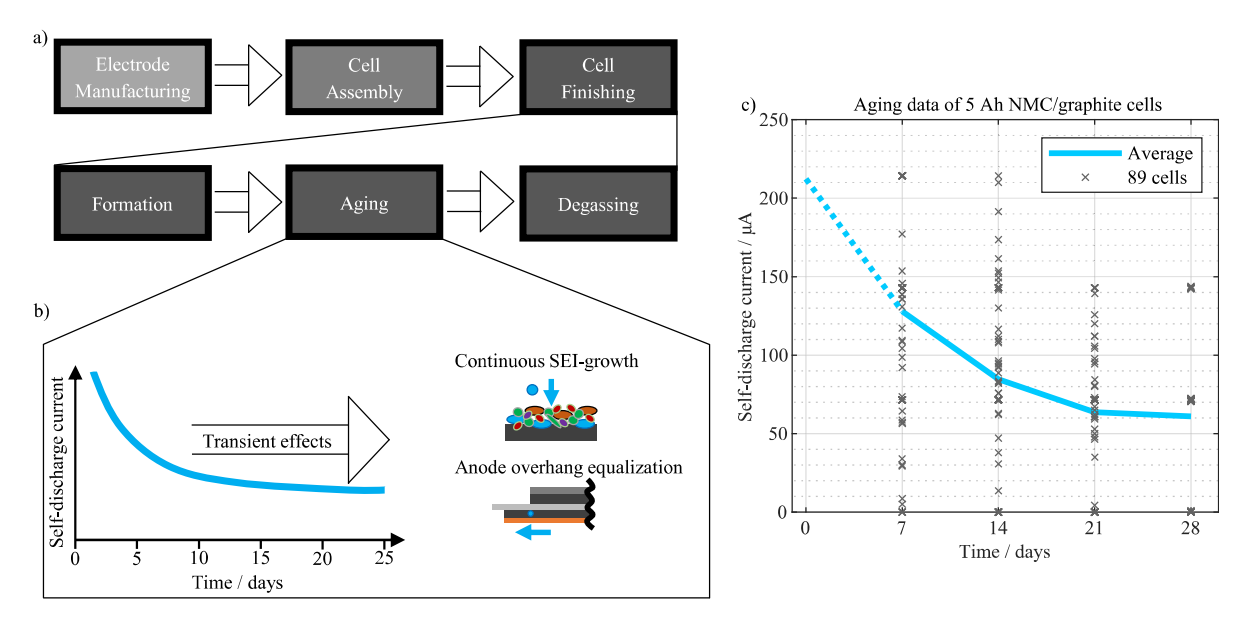
A significant challenge in determining the production and process parameters for lithium-ion battery (LIB) manufacturing is the scaleup from lab to pilot and industrial scale. On multiple occasions, experiments showed differing results when scaled from coin cell level to cylindrical, prismatic, or pouch cell level.<sup>2,3</sup> Some differences might be explained by the geometric anode overhang, which has been shown to cause anomalous behavior like capacity loss or recovery<sup>4–9</sup> and prolonged self-discharge measurements. <sup>10–14</sup> The importance of an anode overhang has been highlighted by multiple sources, <sup>15–17</sup> and the impact on cell performance has been shown in various experiments. <sup>18–21</sup> Most commercial cell designs have geometrically larger anodes and show the anomalous effects of anode overhang equalization to some degree. Even though the effect of the anode overhang is already well documented and present in most commercial cell designs, it is often neglected in the evaluation of formation and aging studies. <sup>2,22–26</sup> Typically, the geometric anode overhang of commercial cells is between 3% to 10%. 5,10,27,28 However, some formation studies were performed with an anode overhang of more than  $20\%.^{24,25}$  Roth et al. showed that an imbalance between the concentration of the active and inactive anode could lead to substantial and transient equalization currents after prolonged storage at a low state-of-charge (SOC). 13 Azzam et al. investigated multiple commercial cylindrical cells and attributed the transient behavior of the self-discharge measured in the range of 5 to 30 d to the anode overhang equalization processes. Before the formation, the active and inactive anode condition is fully delithiated. Therefore, it must be presumed that the highest equalization currents due to the anode overhang occur just after charging the cell for the first time, hence during and after the formation step. However, it was reported that the first cycle capacity loss differed between cell formats. Lee et al. compared various cut-off voltages during formation at coin cell and cylindrical cell levels and found that the capacity retention at 3.6 V was lower only for the cylindrical cells.<sup>2</sup> Bridgewater et al. compared the capacity loss of the first few cycles between coin cells, single-layer, and stacked pouch cells and found that the stacked pouch cells with larger overhang areas lost more capacity.<sup>3</sup> Gyenes et al. attributed the lower first cycle efficiency of fresh commercial cells, at least partially, to the anode overhang equalization. Consequently, the anode overhang equalization processes should not be neglected when conducting experiments on a lab scale to derive process parameters on a pilot or an industrial scale. A suitable solution is the usage of single-layer pouch cells, which offer a compromise between geometric design and ease of use for lab scale.

Figure 1a shows the main LIB production steps: electrode manufacturing, cell assembly, and cell finishing. Along the complete LIB production, the parameters of each production step are controlled to ensure the quality of manufactured cells. The final and most crucial quality assessment is conducted in the cell finishing step. After the dry cells are filled and wetted with electrolyte, the formation step describes the fresh cells' first electrical charge and discharge cycles. 1,29,30 Typically, the formation is directly followed by the aging step, which includes the final electrical characterization of the LIBs before shipping. 1,29,30 After or during formation, there may also be an additional degassing step for some cell formats to extract unwanted gas, which may build up due to side reactions during the first cycles. 30

During cell aging, the cell's capacity, internal resistance, and self-discharge rate are determined. The most time-consuming step during cell aging is the self-discharge measurement, which may take from two to four weeks. <sup>1,29,30</sup> The long cell aging duration is due to the distinct transient behavior of the self-discharge rate. Figure 1b schematically shows the transient self-discharge current and possible underlying mechanisms causing it: Continuous solid electrolyte interphase (SEI) growth <sup>31–37</sup> and anode overhang equalization <sup>10,13</sup> are known to cause transient effects as well as contribute to the self-discharge of LIBs. The equalization processes of the anode can also occur in the active anode, where inhomogeneity of lithium distribution <sup>12,38</sup> may similarly change the state of lithiation and, consequently, the cell voltage. Self-discharge is also caused by other side reactions and mechanisms, like electrolyte oxidation, <sup>32,39</sup> redox shuttle processes, <sup>39–41</sup> and soft short circuits. <sup>17,42,43</sup> However, these mechanisms might or might not show a transient behavior themselves

The investigation of reversible self-discharge, like redox shuttles or electrolyte oxidation, is mainly conducted at higher cell SOCs or voltages. 44-49 The reason for the preference for higher voltages is the

<sup>&</sup>lt;sup>2</sup>University of Münster, MEET Battery Research Center & Helmholtz Institute Münster (IEK-12), Forschungszentrum Jülich, 48149 Münster, Germany



**Figure 1.** (a) Overview of the main lithium-ion battery production steps. (b) Illustration of the typical transient self-discharge measured during the aging step and the underlying mechanisms. (c) Exemplary self-discharge measurements during aging of 89 pilot scale 5 Ah NMC622/graphite cells, further details in supplemental S1.

dependence of the side reactions on the combination of the stable electrolyte voltage window and the cathode potential.<sup>50,51</sup> This combination was shown to govern the reversible self-discharge current. 45,48,49 Therefore, measuring cells at low to moderate SOCs might reduce the impact of cathode-driven side reactions, which is supported by the reversible and irreversible capacity loss and endpoint slippage analysis from Keil et al.,<sup>52</sup> Streck et al.<sup>53</sup> Jagfeld et al. 54 Keil et al. analyzed the endpoint slippage of NCA/ graphite cells and found that cathode-driven side reactions were moderate or small for storage SOCs up to 80%. 52 Streck et al. showed for NMC/silicon-graphite cells that the reversible selfdischarge or the coupled side reactions were low compared to contributions from anode side reactions at SOC of 50% and below. Jagfeld et al. observed a similar trend that was more pronounced with high-energy cells than high-power cells, where the contribution of coupled side reactions was generally higher.<sup>54</sup> While the individual contributions of the underlying mechanisms to the transient self-discharge are not yet fully understood, the continuous SEI growth and anode overhang equalization are confirmed to show a transient behavior. In the scope of this work, these two effects are presumed to be the main causes for the observed transient effects.

In the context of cell aging during production, minimizing side reactions and transient self-discharge could help to identify manufacturing defects like soft shorts, which are not as dependent on the cell voltage as side reactions. The transient self-discharge is also observed in scaled-up LIB, as shown in Fig. 1c. The average selfdischarge current over all 89 NMC622/graphite pouch cells shows the expected transient self-discharge behavior. In the first week, the self-discharge current averages at around 130  $\mu$ A but decreases to  $60 \,\mu\text{A}$  after four weeks. Additional information on the cell specification, formation, and aging of Fig. 1c is available in supplemental S1. When determining cell quality via a self-discharge measurement, measuring the actual cell quality is essential instead of transient effects. For similar long-term stored NMC622/graphite pouch cells from the same manufacturer, Roth et al. showed self-discharge currents between 10 to 50  $\mu$ A during four weeks of measurement. Therefore, differences in cell quality of a similar magnitude would be difficult to evaluate after formation. A better understanding of transient self-discharge can improve quality evaluation during the cell aging step and help optimize the self-discharge measurements for faster and more reliable characterization.

In the context of cell formation during production, a fast formation protocol is desirable while maintaining cell

performance, which is often linked to a high-quality SEI layer. The mechanism behind SEI growth and its dependence on the graphite potential has been extensively studied in the literature. 35,55,56 However, the interplay of anode overhang and cell voltage is rarely considered in studies regarding SEI and formation. Broussely et al. investigated the capacity loss for various large format cells at voltages of 3.8 V, 3.9 V, and 4.0 V and found no significant impact of storage voltage on capacity retention. Lee et al. showed that the voltage range during formation had a minor effect on half-cell and coin cell levels. This changed for cylindrical cells with anode overhang, where capacity retention was worse at 3.6 V. Germain et al. investigated the cut-off voltage during formation for large format 50 Ah cells with approximately 8% anode overhang and found the capacity losses to be similar for different cut-off voltages. Drees et al. investigated five formation procedures with varying cycle times and found no significant quality differences between fast and slow formation as long as lithium plating was prevented. 26

These results contrast formation studies with extended periods in the high voltage range during formation, where improved cell capacity retention was reported. Weng et al. reported a small but highly reproducible positive impact of fast formation in the high voltage range on the cycle life of 2.36 Ah stacked pouch cells. Similarly, Müller et al. presented a highly positive effect of a constant voltage (CV) charging step with C/50 cut-off voltage on the cycle aging performance of 2 Ah stacked pouch cells. These findings are interesting regarding the anode overhang in so far that both stacked pouch cell formats used double-side coated electrode sheets. In both cases, these led to more than 20% anode overhang 24,25 due to the outermost electrode sheet without a cathode counterpart.

This work aims to investigate the impact of the anode overhang on the transient self-discharge rate during the cell aging step of lithium-ion cells. Separating the effect of anode overhang from SEI growth is achieved by utilizing single-layer pouch cells with varying anode sizes. The transient self-discharge behavior is studied at different SOCs to compare the SEI growth and anode overhang equalization at different conditions. The implication of the results on the formation and cell aging step is given. All cells were exposed to a short calendar and cycle aging phase to qualitatively evaluate the cell performance for different SEI growth during storage. The primary content of this paper is divided into two sections: an experimental section and a results and discussion section.

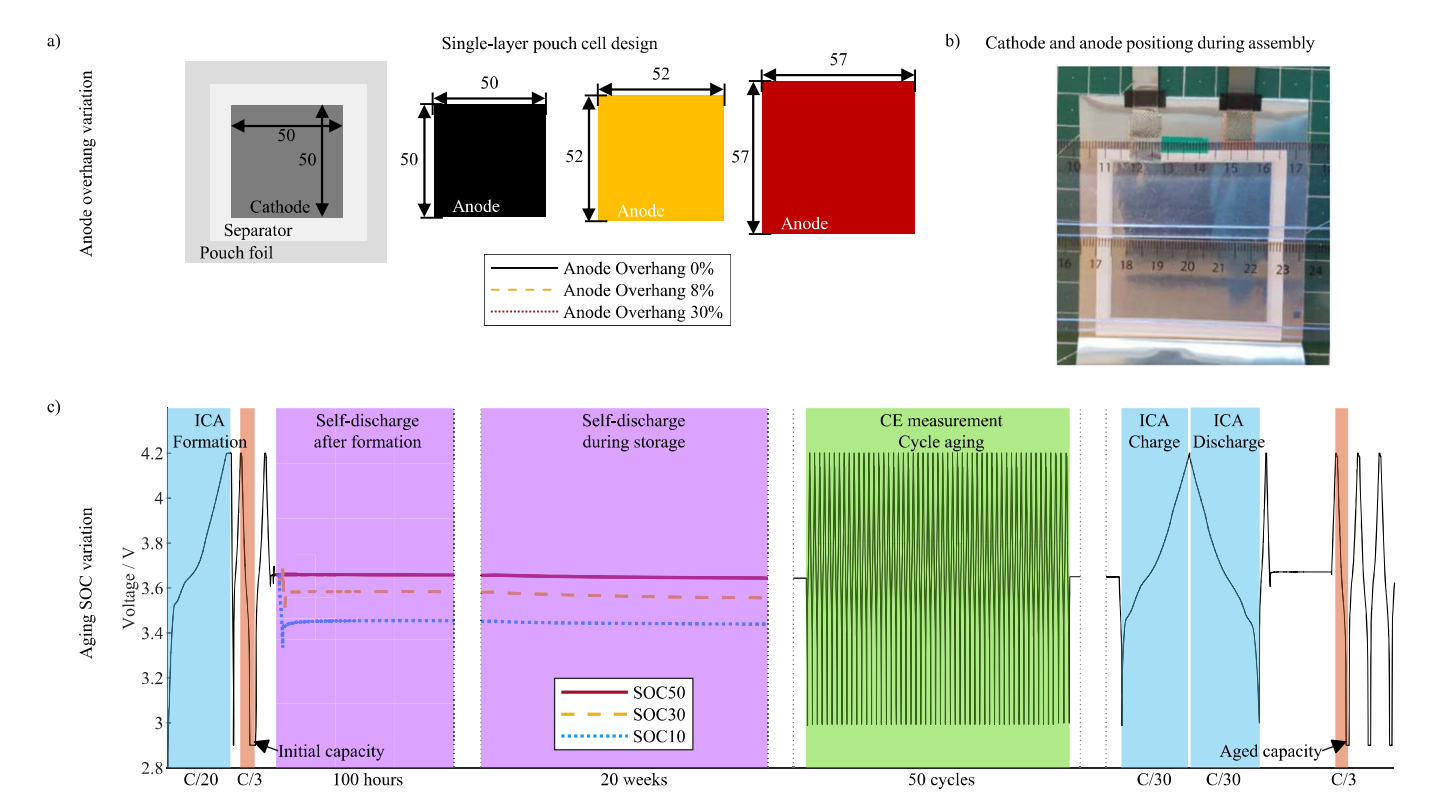


**Figure 2.** Overview of the experiment: (a) Single-layer pouch cell design with different anode dimensions in mm, further referred to as 0%, 8%, and 30% overhang cells. (b) Example of the cathode to anode positioning of an 8% overhang cell, where the 1 mm overhang of the anode can still be seen through the thin separator layer. (c) Schematic of full measurement protocol: Initial formation with a C/20 charge, initial capacity measurement in the second cycle, self-discharge measurement by voltage decay method for 100 h followed by further 20 weeks, cycle aging for 50 cycles at C/3, ICA and DVA evaluation by a C/30 cycle, and final aged capacity measurement.

#### **Experimental**

*Cell setup.*—The cells used in this study are 18 single-layer pouch cells with single-side coated electrodes. The electrode material was supplied by the MEET Battery Research Center. The positive active material consists of a BASF Li[Ni $_{0.6}$ Mn $_{0.2}$ Co $_{0.2}$ ]O $_{2}$ (NMC622) and the negative electrode is a graphite-based Hitachi SMG-A5. The electrode properties are presented in Table I. A Celgard Q16S1HI with 16  $\mu$ m thickness was used as a separator. The cells were filled with 1 M LiPF $_{6}$  in EC:EMC 3:7 wt% without further additives and vacuum sealed.

Figure 2a shows the cell setup and the dimensions of the single-side coated electrode sheets. The cathode sheet of all 18 cells was  $50 \times 50 \text{ mm}^2$ , and the separator was  $60 \times 60 \text{ mm}^2$ . Three different anode geometries with six cells per setup were cut from the manufactured graphite sheets:  $50 \times 50 \text{ mm}^2$ ,  $52 \times 52 \text{ mm}^2$ , and  $57 \times 57 \text{ mm}^2$ . The different cell setups led to an anode overhang of 0%, 8%, and 30%, respectively. Figure 2b shows the stack positioning of an 8% overhang cell. The thin and transparent separator allows a precise cathode stack positioning to achieve equivalent overhang length in all cells. This is especially crucial for the cells with 0% overhang, where cathode overlap may lead to fast degradation and capacity fade. Even if the electrode positioning

Table I. Electrode properties.

Electrode	Cathode	Anode
Current collector Porosity Coating thickness Active material mass loading Theoretical specific capacity Specific areal capacity	Copper—6 μm 30% 66 μm 19.2 mg cm <sup>-2</sup> 179.7 mAh g <sup>-1</sup> 3.45 mAh cm <sup>-2</sup>	Aluminum—10 μm 30% 77 μm 11.1 mg cm <sup>-2</sup> 372 mAh g <sup>-1</sup> 4.13 mAh cm <sup>-2</sup>
Specific areas cupacity	erre in the em	

had not been 100% perfectly aligned in this study, no increased degradation or capacity decrease was observed in subsequent testing of the cells with 0% overhang. The nominal capacity of the cells was 80 mAh, corresponding to approximately 155 mAh g $^{-1}$ , and was used for all anode overhang sizes.

Measurement protocol.—The full measurement protocol is presented schematically in Fig. 2c. After vacuum sealing, all cells were cycled with the same formation protocol. First, all cells were charged with constant current constant voltage (CCCV) at C/20 to 4.2 V until a C/100 cut-off was reached. Then the cells were discharged at 1 C to 2.9 V. This is followed by a full CCCV cycle at C/3 with a cut-off after reaching the C/20 end criterion while measuring the initial discharge capacity. Then the cells are charged again and discharged at C/3 to a defined SOC based on the initial discharge capacity, as depicted in Fig. 2c. Two cells of each anode overhang geometry are discharged to a capacity-defined SOC of 50%, 30%, and 10%, respectively, and a resting period for selfdischarge evaluation commences. The cell voltage is measured over the first 100 h of the resting period until the formation protocol concludes. After formation, the cell voltage was continuously measured weekly over 20 weeks (3600 h) during calendar storage at the respective SOC. After storage, all cells were constant current (CC) cycled at C/3 between 3.0 V and 4.2 V for 50 cycles. Apart from cycle aging, coulombic efficiency (CE) was additionally determined. A slow C/30 charge and discharge were performed to determine the open circuit voltage (OCV) for incremental capacity analysis (ICA) as well as differential voltage analysis (DVA). Finally, the aged capacity was measured in full CCCV cycles at C/3 with a cut-off after reaching a C/20 end criterion.

For the formation protocol, an HRT-M high-resolution battery tester from Battery Dynamics and a BaSyTec CTS were used. The HRT-M offers an improved voltage resolution of 1  $\mu$ V for analyzing the voltage drop during the first 100 h. In comparison, the CTS

offers a voltage resolution of 0.3 mV. The initial capacity and the first 100 h of self-discharge data of the cells with 0% overhang stored at SOC30 and SOC10 could not be retrieved. One SOC10 cell with 0% overhang was afterward stored at a different SOC and excluded from further evaluation. The weekly voltage measurement during calendar storage was conducted manually with a Hameg HM8112 precision multimeter with 6 1/2 digits. The cycle aging, ICA, and aged capacity measurements were performed with the BaSyTec CTS. All measurements, including the calendar storage, were performed in a climate chamber at 25 °C.

While Fig. 2c is only a schematic of the full test protocol, it must be emphasized that special care was taken to always perform the vacuum sealing, the formation protocol, and the calendar storage for all cells in the same temporal sequence. This was done to ensure a similar evolution of the transient effects in the cells and allow for as much comparability as possible.

*Voltage decay method.*—The method for determination of the self-discharge current during the first  $100\,\mathrm{h}$  after formation and the 20 weeks of storage is the voltage decay method described by Roth et al. and Streck et al.  $^{13,53}$  The measured decay in the cell voltage dV over the corresponding storage duration dt is multiplied by the differential capacity dQ/dV, resulting in the self-discharge current  $I_{VD}$ , as shown in Eq. 1:

$$I_{VD} = dQ/dV \cdot \frac{dV}{dt}$$
 [1]

Streck et al. showed that the results of voltage decay and voltage hold methods are comparable, especially when the differential capacity dQ/dV was determined via ICA at the specific storage cell voltage.<sup>53</sup> Therefore, in this work, the voltage decay method in

combination with a dQ/dV value from the ICA of the C/20 formation curve was used to calculate the self-discharge current  $I_{VD}.$  The dQ/dV value on the curve was determined by the corresponding cell voltage at the end of the first 100 h after formation. For the 20 weeks calendar storage, the dQ/dV was determined with the weekly measured cell voltage of each individual cell.

#### **Results and Discussion**

Differential capacity.—The initial voltage window or electrode balancing is defined by the ratio of negative to positive electrode capacity (n/p ratio). According to the specific areal capacity in Table I, the n/p ratio of the cells is 1.2. The n/p ratio affects the endof-charge and end-of-discharge potentials, <sup>58</sup> as well as the location of peaks in ICA and DVA curves. Per definition, the n/p ratio is based on the mass loading or specific capacity of each electrode, which means that it is not affected by the geometric anode overhang size. Figures 3a-3c show the ICAs for the C/20 formation and the C/ 30 slow charge and discharge after aging for three cells of each overhang. The ICA of the formation process in Fig. 3a shows that the peaks for different anode overhang geometries are very close in position and height. This suggests that the initial voltage window of the cells is still similar regardless of the geometric anode overhang. In Figs. 3b and 3c, the peaks of the aged cells are shifted to higher potentials for the cells with larger anode overhangs. Additionally, the differential capacity peaks are overall lower for the aged cells. These results indicate that the voltage window of the aged cells already changed, which can be caused by the loss of lithium inventory.<sup>58</sup> Figures 3d–3f show a similar shift for larger overhangs in the DVA results. The central graphite peak is shifted to the right after aging and with increasing overhang size. This shift is plausible since both aging and larger overhang  $^{T}$  will lead to lower lithium

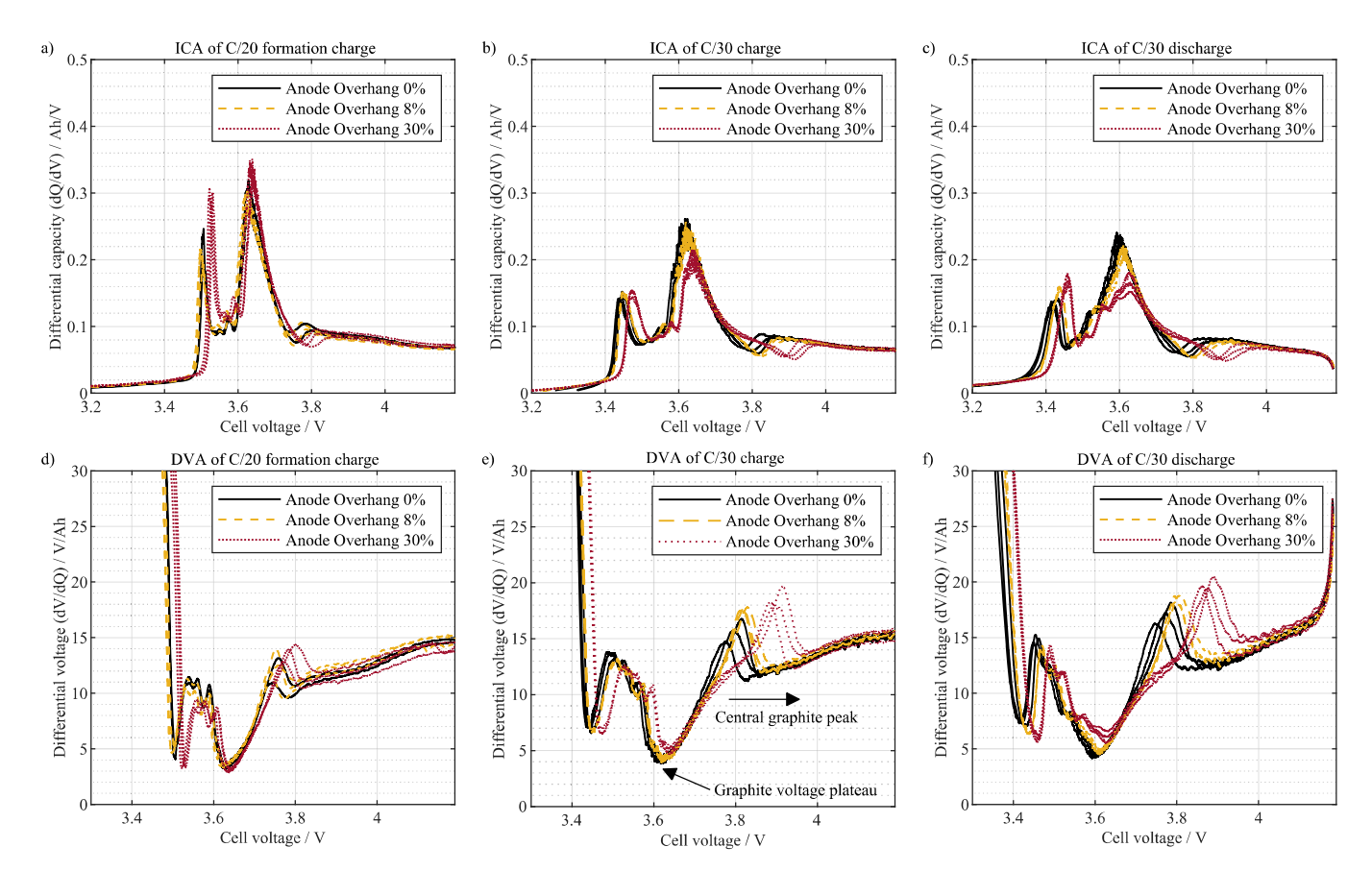


**Figure 3.** Incremental capacity analysis of the (a) C/20 formation charge, (b) C/30 charge after aging, and (c) C/30 discharge after aging. Differential voltage analysis of the (d) C/20 formation charge, (e) C/30 charge after aging, and (f) C/30 discharge after aging. The curves and peaks are still uniform during formation for different anode overhang sizes. After aging, the peaks for larger anode overhang are shifted, indicating less available lithium inventory in the full cell. dQ/dV values from the C/20 formation charge are used to evaluate the self-discharge.

inventory in the active anode. Consequently, the anode voltage window will increase compared to the cathode voltage window, 52 causing a shift of the central graphite peak to higher full-cell voltages, as was already shown for aged cells. 27 Even though the geometric anode overhang has little impact on the initial voltage window, it was shown that the overhang could cause a significant shift in the voltage window after calendar and cycle aging.

As stated in the experimental section, the differential capacity dQ/dV from Fig. 3a was used to calculate the self-discharge current with the voltage decay method given in Eq. 1. Figures 3a-3c show that there is a difference between using the dQ/dV from the ICA of the formation cycle or from the ICAs after aging. For a singular selfdischarge measurement, the difference in dQ/dV of the formation or aged ICA curves is minor. As mentioned above, the dQ/dV values of the aged ICAs are generally slightly lower and shifted for different anode overhangs, as shown in Figs. 3b and 3c. In contrast, the dQ/ dV values in Fig. 3a are more uniform over the different anode overhang sizes. From a time perspective, the formation is closer to the beginning of the self-discharge measurements, which causes the dQ/dV values to resemble this state better than the aged condition. Schomburg et al. also used the initial C/20 formation to evaluate the DVA of cells to characterize SEI growth, 61 and they stated assumptions for the validity of using the DVA during initial formation. Due to the uniform ICA curves in the initial condition, the C/20 formation curve was used for further self-discharge evaluation.

In summary, the voltage window changes significantly from the initial to the aged condition. The geometric anode overhang contributes to the changing voltage window, which can be seen as a shift of the peak positions in ICA and DVA curves.

Self-discharge after formation.—After two formation cycles, the cells are discharged to the determined SOCs. Figures 4a–4c show the voltage development for the first 100 h after formation. All cells

show short-term voltage relaxation, <sup>13,62</sup> which is visible at SOC10 for more than 20 h. In contrast, the voltage of the cells at SOC30 and SOC50 changes earlier into a downward slope. Overall, the voltage range is around 3.45 V for SOC10, around 3.57 V to 3.59 V for SOC30, and around 3.65 V for SOC50. The biggest spread is at SOC30, where the voltage curves are the most distinct for the anode overhang of 8% and 30%. Figures 4d–4f show the calculated self-discharge current for each SOC.

At SOC10 in Fig. 4d, the self-discharge current stabilizes after around 50 h below 1  $\mu$ A regardless of overhang size. Furthermore, the self-discharge current seems almost stable without a strong transient phase after 50 h. In Fig. 4e at SOC30, the self-discharge current, similar to the voltage decay, shows distinct curves for 8% and 30% anode overhang. The larger 30% overhang led to a measured self-discharge current in the range of 5 to 10  $\mu$ A, whereas the smaller 8% overhang showed a lower self-discharge current in the range of 1 to  $2 \mu A$ . Figure 4f shows that at SOC50, apart from the first 20 h, where voltage relaxation is not yet fully finished, the self-discharge current is overall very similar regardless of anode overhang and is still decreasing from 10 to  $5 \mu A$ . The literature showed that the long-term or steady-state self-discharge current of LIB between 3.5 V and 3.7 V can be in a close range. <sup>12,63</sup> This could explain the similar range of the self-discharge current between SOC30 and SOC50 for the 30% overhang cells. Contrary to expectations from the results at SOC30, the anode overhang equalization seems not dominant at SOC50. Specifically, the cells with 0% anode overhang show the same trend, which indicates that the transient effect from approximately 30 to 100 h is most likely caused by SEI growth. Attributing the increase in self-discharge current at cell voltages above 3.6 V to SEI growth is in line with work from Lee et al. <sup>2</sup> and German et al. <sup>57</sup> Both reported incomplete SEI growth below 3.6 V. <sup>2,57</sup> Broussely et al. already remarked that SEI growth should occur according to the voltage plateaus of graphite.<sup>31</sup> Consequently, before reaching the graphite voltage

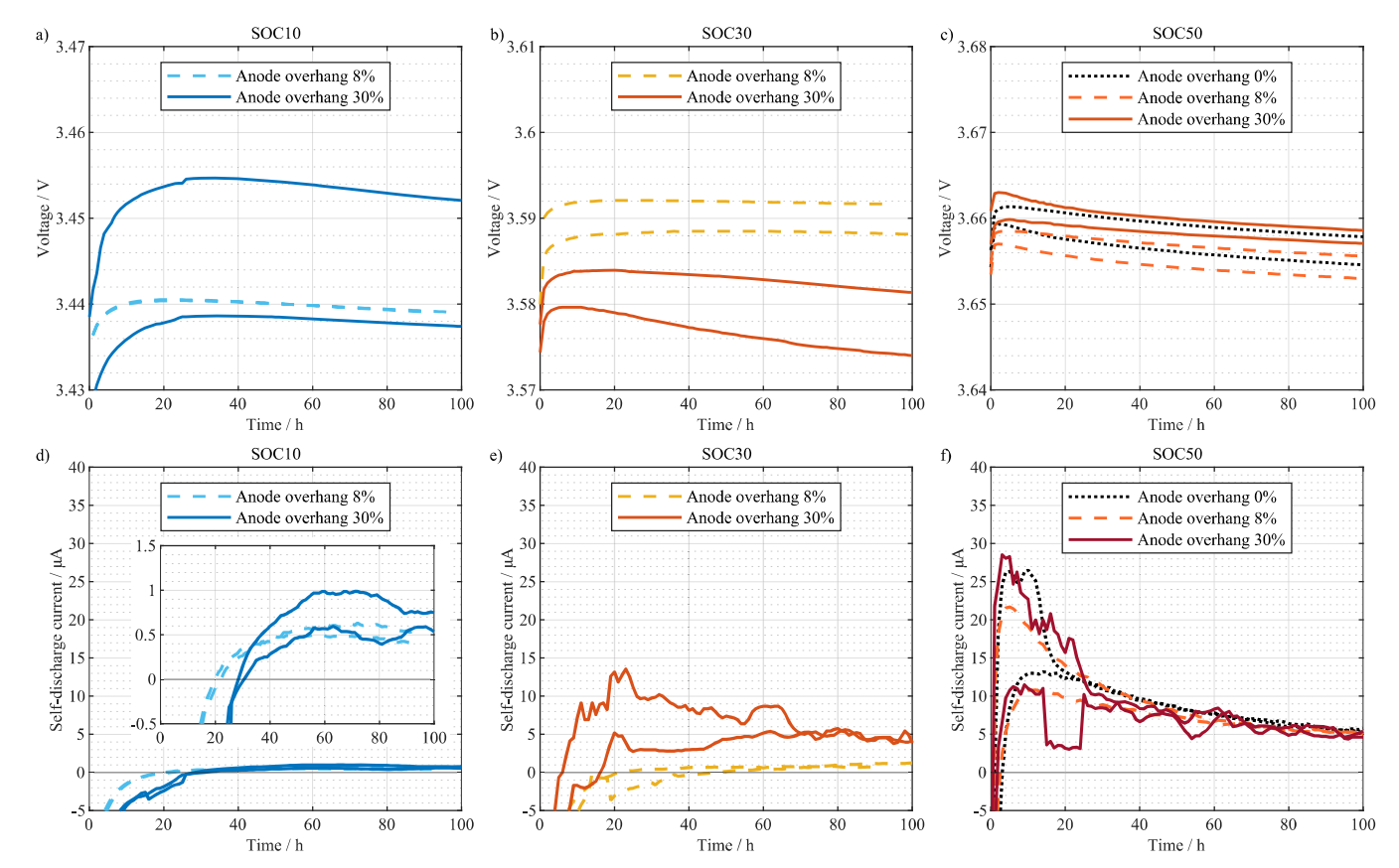


**Figure 4.** Voltage development for the first 100 h after formation (a) at SOC10, (b) at SOC30, and (c) at SOC50. Calculated self-discharge via voltage decay method for the first 100 h after formation (d) at SOC10, (e) at SOC30, and (f) at SOC50. The data of the cells with 0% overhang stored at SOC10 and SOC30 could not be retrieved.

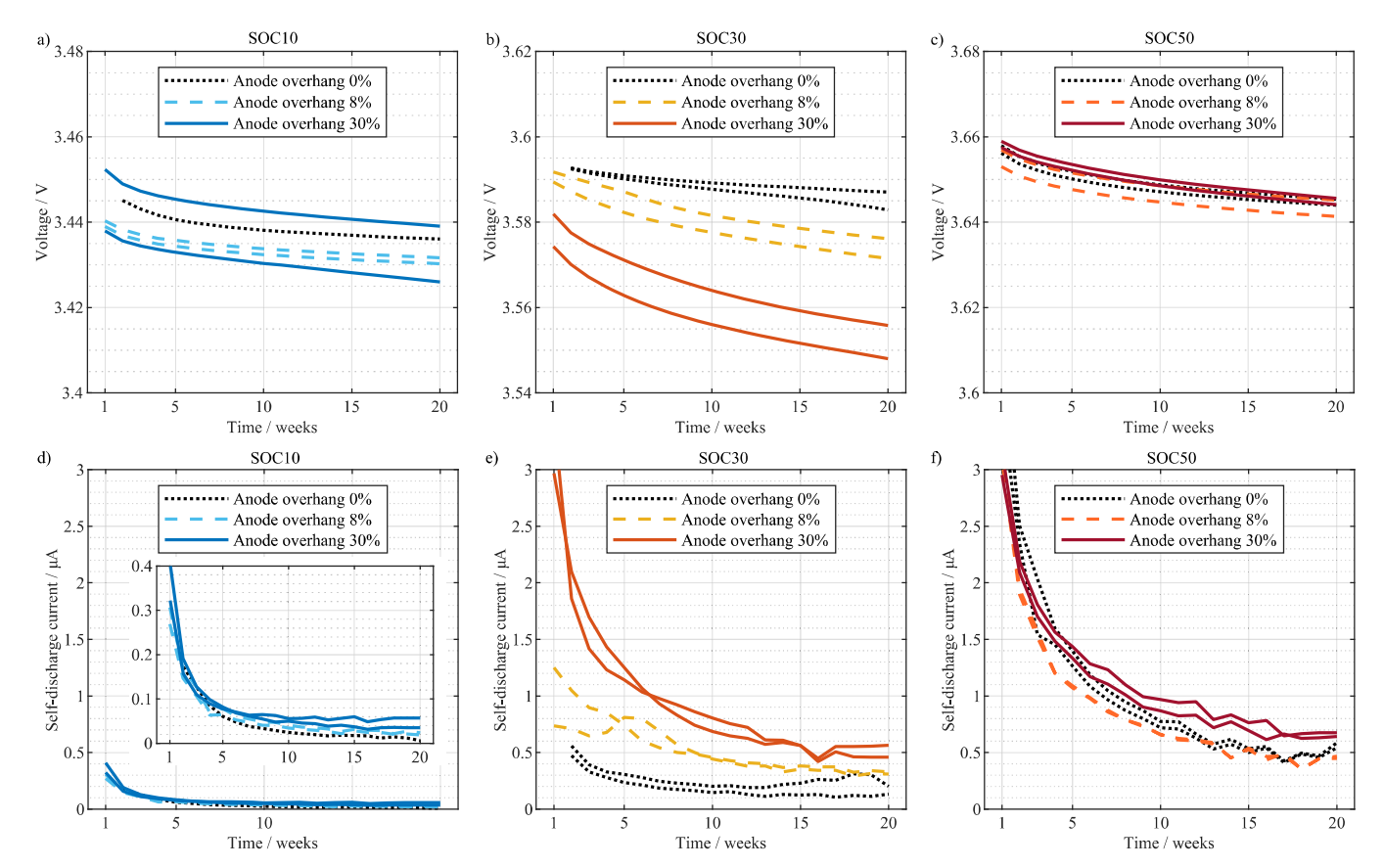


Figure 5. The weekly voltage measurement for 20 weeks during calendar storage (a) at SOC10, (b) at SOC30, and (c) at SOC50. Calculated self-discharge via voltage decay method for 20 weeks during calendar storage (d) at SOC10, (e) at SOC30, and (f) at SOC50.

plateau, the change in SEI growth may be more pronounced. The investigated NMC622 and graphite material combination was also used by Münster et al., where a 3-electrode cell containing a Lireference showed that the voltage above 3.6 V marks the transition to the graphite voltage plateau. <sup>64</sup> In Figs. 3d–3f, the minimum of the differential voltage dV/dQ above 3.6 V in the DVA marks the transition to the graphite voltage plateau for the investigated cells. Therefore, SEI growth should be sensitive to the cell voltage around and above 3.6 V. Additionally, the anode overhang size affects the graphite potentials, shown by the shift of the peaks in the DVA curves in Figs. 3d–3f.

Self-discharge during storage.—The weekly voltage measurement for all cells is shown in Figs. 5a-5c. The overall voltage ranges of each SOC are still in the same range as in Figs. 4a-4c. Figures 5d -5e show the self-discharge current calculated via the voltage decay method with dO/dV values from the ICA of Fig. 3a. The selfdischarge current at SOC10 is still not fully stable after the first 100 h but instead further decreases over the entire measurement time of 20 weeks, as shown in Fig. 5d. Although the different anode overhang sizes have a small effect on the self-discharge current, a ranking from 0% to 8% to 30% overhang can still be observed. The final measured self-discharge current is well below  $0.1 \,\mu\text{A}$  at SOC10. At SOC30 and SOC50, the transient self-discharge, as described in Fig. 1c, is prominently shown. Like the first 100 h, the anode overhang equalization remains dominant at SOC30 over the calendar storage, shown in Fig. 5e. The first five weeks exhibit the largest discrepancy between the overhang sizes, but even after 20 weeks, the almost stable self-discharge current is still ranked from 0% to 8% to 30% overhang. This is the opposite of the voltage ranking in Fig. 5b, which suggests that SEI growth below 3.6 V was still a minor factor. This notion is supported by the weak transient phase of the 0% overhang cells in Fig. 5e. The calendar storage at SOC50 also continues the trend of the first 100 h, which is shown in

Figs. 5c and 5f. The voltage and the self-discharge current curves are close regardless of overhang size, showing a strong transient trend. After approximately twenty weeks, the cells with 30% overhang show a self-discharge current of around 0.65  $\mu$ A, which is slightly higher than 0.5  $\mu$ A of the 0% and 8% cells. As was proposed in the literature, <sup>12,13,34</sup> if the continuous SEI growth contributes to the self-discharge, then a 30% larger graphite anode would also increase the self-discharge current by 30%, which fits the observed values.

In summary, for the SOC10 measurement, a reliable self-discharge current in the range of 1  $\mu$ A ( $\sim$ C/80.000) could be determined within 50 h. However, the final self-discharge current of the cells at SOC10 was in the range of 0.02  $\mu$ A ( $\sim$ C/4.000.000), which was still decreasing after more than 20 weeks. At SOC30 and SOC50, the measured self-discharge current was magnitudes higher even after 20 weeks of measurement. Consequently, self-discharge measurements at lower SOCs might be more sensitive to soft shorts or cell defects, allowing for faster detection of anomalous cell behavior.

SEI growth and anode overhang.—Figure 6a compares the selfdischarge current during storage for the 0% and 30% overhang cells at each SOC. The inhomogeneity of lithium distribution should be low after only two formation cycles, <sup>38</sup> and the equalization processes in the active anode should be concluded after more than one week.<sup>6</sup> Additionally, if cycling would have caused inhomogeneity of lithium distribution, then a capacity recovery effect and voltage increase due to relaxation would be expected during rest periods. Reversible shuttle processes and electrolyte oxidation should also be low at moderate cell voltages, which is shown by the reduced amount of cathode and coupled side reactions below 3.7 V. Consequently, for the cells with 0% anode overhang, it is presumed that the transient self-discharge was predominantly coming from continuous SEI growth. The data from Fig. 6a is used to calculate the deviation in self-discharge current between the 0% and 30% overhang cells, shown in Fig. 6b. Here, the averaged self-discharge

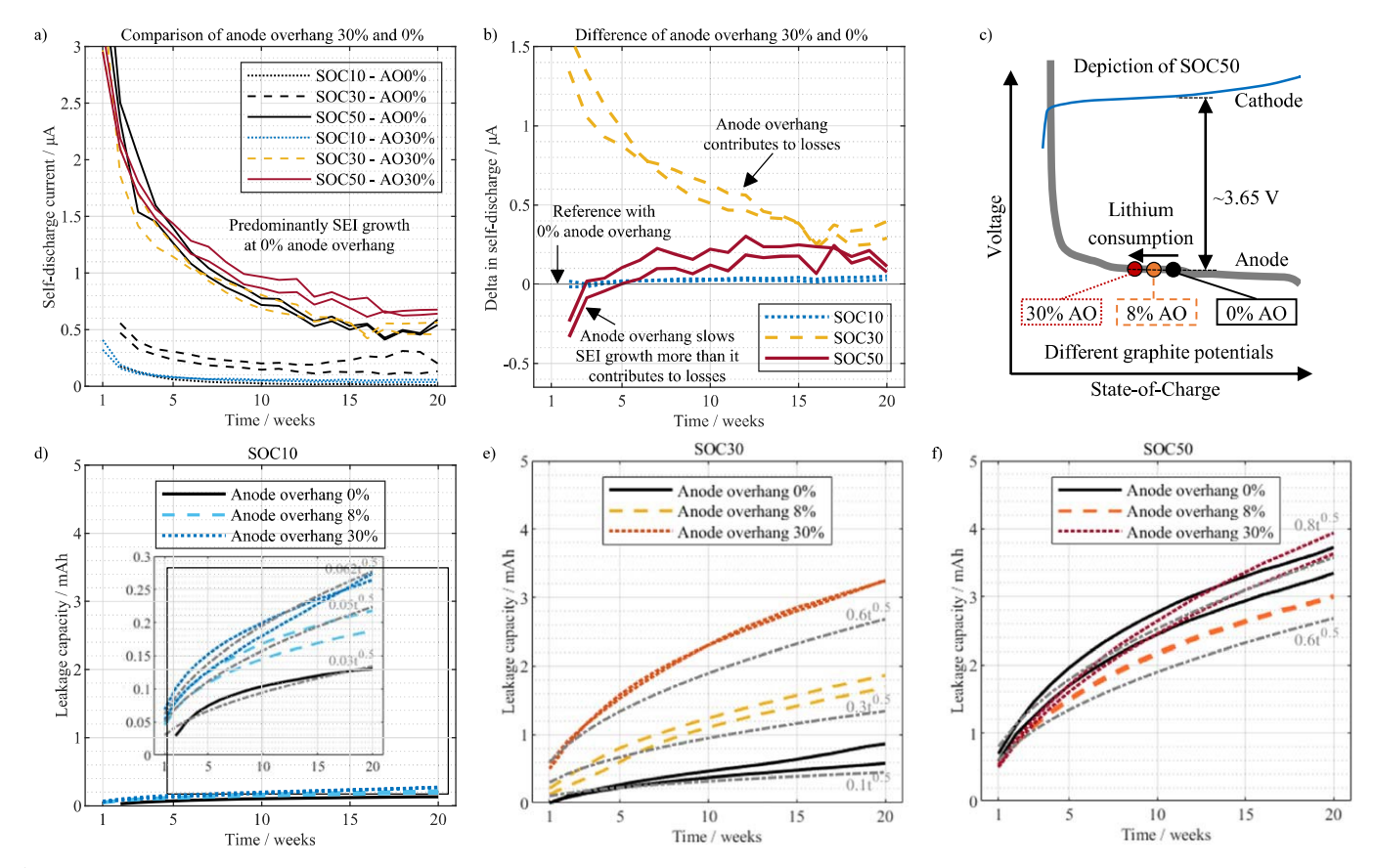


**Figure 6.** (a) Comparison of self-discharge for 0% and 30% overhang cells. For cells without anode overhang, the self-discharge is assumed to be predominantly from SEI growth. (b) Difference between self-discharge of 30% and 0% overhang cells, calculated by subtracting the average self-discharge of the 0% overhang cells. At SOC30, the anode overhang contributes to the measured self-discharge, while at SOC50, the anode overhang seems to slow down the SEI growth initially. A schematic explanation is depicted in (c) for SOC50, where the lithium consumption due to the anode overhang changes the graphite potential, which governs the SEI growth rate. Cumulative leakage capacity (d) at SOC10, (e) at SOC30, and (f) at SOC50 for different overhang cells show good agreement with approximated  $t^{0.5}$  power law curves. The discrepancy between the power law curve to the measured leakage capacity curves could be interpreted as the contribution of the anode overhang to the leakage capacity.

current of the 0% overhang cells was subtracted from the 30% overhang cells. The anode overhang barely contributed to the selfdischarge current at SOC10 but started to cause additional capacity loss at SOC30. This would be the expected trend for a larger anode overhang from the literature.<sup>8,10</sup> This trend was not observed at SOC50, where the effect of the anode overhang was apparently lower and slowed down. The reason for this apparent slowdown might be the actual graphite potential changing. The overhang areas drain lithium from the active graphite anode, causing the graphite potential to increase. In Fig. 6c, the notion of different graphite potentials due to lithium consumption of the anode overhang at SOC50 is schematically depicted. Attia et al. and Köbbing et al. also reported a deviation from the typically proposed simple square-root dependence on time  $(t^{0.5})$ . 36,66 Attia et al. already mentioned overhang effects, among other factors, potentially convoluting the SEI growth measurements.<sup>36</sup> Köbbing et al. described how SEI growth causes lithium consumption in the graphite anode and increases the graphite anode potential, which then slows down further SEI growth. 66 As described above, this is essentially the same effect the lithium movement into the anode overhang would have on the graphite potential and could explain the trends shown in Fig. 6b. This notion is further supported by the strong dependence of SEI growth or self-discharge on the anode potential, as shown for glassy carbon,<sup>33</sup> graphite,<sup>67</sup> and silicon<sup>68</sup> anodes. Furthermore, the DVA curves in Figs. 3d–3f show a shift of the central graphite peak depending on the anode overhang size, confirming that the graphite potentials differ.

The results from the self-discharge during the 20-week storage certainly support the idea of a  $t^{0.5}$  dependency of the SEI

growth.32,35,36 The cumulative leakage capacity at each SOC with approximated  $t^{0.5}$  power law curves is shown in Figs. 6d-6f. At SOC10 in Fig. 6d, the leakage capacity is in good agreement with the approximated  $t^{0.5}$  power law curves. Presumably, the impact of anode overhang equalization is low, and the main contribution to selfdischarge at SOC10 may come from SEI growth. Still, the SEI growth may also be occurring in the anode overhang. Therefore, increased SEI growth for geometrically larger anodes is expected, which explains the dependency on the anode overhang seen in Fig. 6d. At SOC30 in Fig. 6e, the cumulative leakage capacity shows an even stronger dependency on the anode geometry. The  $t^{0.5}$  dependency generally underestimates the capacity loss of the 8% and 30% overhang cells. This is in line with the results from Attia et al., where the fitted powerlaw exponents for calendar storage of cylindrical cells with anode overhang were above 0.5. 36 As also shown in Fig. 6b, the additional capacity loss could be attributed to the anode overhang. In contrast to SOC10 and SOC30, the cells at SOC50, shown in Fig. 6f, do not show a clear dependency on the anode overhang. However, as explained above, the expected capacity loss due to larger anode overhang areas should be even more pronounced at SOC50 than at lower SOCs. This is not the case, which is a further indicator, that even though the cell voltages in Fig. 5c are quite similar, the actual graphite potentials are different for 0%, 8%, and 30% overhang cells at SOC50. Therefore, separating the leakage capacity into contributions from SEI growth and anode overhang is difficult at SOC50. Assuming the approximated  $t^{0.5}$ power law curves are in good agreement with the SEI growth, then the discrepancy of the power law curve to the measured leakage capacity curves could be interpreted as the contribution of the anode overhang to the leakage capacity.

In summary, these results indicate that the reversible lithium movement from the anode overhang changes the graphite anode potential, which can affect the SEI growth rate. Then the question is whether the SEI growth rates at different SOCs affect the cell performance.

Coulombic efficiency.—All cells were cycled 50 times between 3.0 V and 4.2 V with a constant rate of C/3 without CV criterion. The CE was determined by dividing the discharge capacity by the preceding charge capacity of each cycle. It must be noted that the BaSyTec CTS system has a lower current and voltage resolution, which can cause measurement deviations and errors. In supplemental S2, a CE study comparing the high precision HRT-M device and the CTS was conducted on commercial 18650 cells, and a measurement error was identified for the CTS. The CE of the pouch cells showed a similar behavior as described in supplemental S2, where the CE of some cells stabilized at values above one. Anomalous CE values above one were also reported for cells stored at moderate to high SOCs in combination with anode overhang areas.<sup>4,5</sup> In both studies, the CE stabilized closely below one after sufficient cycling, which was not true for some investigated cells. For the CE evaluation of the investigated cells, the focus is not on quantifying the stabilized CE cycles but on the clear differences during the first few cycles. For better readability, the CE values have all been offset to unity for the very last of the 50 cycles. The original CE values are included in supplemental S3 and show a similar trend for the first few cycles.

The CE of one cell for each anode overhang and SOC are shown in Fig. 7. In Fig. 7a, cells with 0% overhang show a significantly lower CE only for the first cycle after storage. This capacity loss also correlates to the storage SOC, with higher capacity losses for the storage at SOC10 and SOC30. These results indicate a late formation of SEI that was not performed during the storage below 3.6 V. The SOC50 cells also showed a lower CE for the first cycle, suggesting that SEI was continuing to grow specifically at cell voltages above 3.7 V. In contrast, the 30% overhang cells in Fig. 7c show a more pronounced and storage SOC-dependent behavior, like the anomalous CE reported by Gyenes et al. and Wilhelm et al.<sup>4,5</sup> The storage at SOC50 with large overhang areas shows the mentioned anomaly of CE above one, which is caused by the anode overhang equalization. The opposite effect is visible at SOC10, where additional capacity is reversibly lost into the anode overhang. However, the first cycle at SOC50 in Fig. 7c also shows a lower CE than the subsequent cycles. This is once more a strong indicator of the late SEI growth, as seen for the 0% overhang cells. The 8% overhang cells in Fig. 7b exhibit a behavior that is fairly between the 0% and 30% overhang cells. As mentioned, commercial or industrial scale cells typically have anode overhang areas of 3 to 10%. Wilhelm et al. used industrial scale cells with 10% anode overhang, but the CE curves of the 30% overhang cells were more in line with the results from Wilhelm et al. than the 8% overhang cells of this study.

A reason for this behavior is that for the  $52 \times 52 \text{ mm}^2$  anodes of the 8% overhang cells, the maximum distance from the active to the inactive anode is only 1 mm. For the 30% overhang cells, the maximum distance is 3.5 mm. For the commercial cylindrical cells studied by Wilhelm et al., the anode overhang geometry was more complex, and the maximum distance was 20 mm at the inner end of the jelly roll and 60 mm at the outer end. Anode overhang equalization would take far longer at these distances, which explains the better CE agreement between the cylindrical cells and the 30% overhang cells.

Overall, the CE measurements show a capacity loss for the first cycle after formation and calendar storage, indicating further SEI growth. After the first cycle capacity loss, the measured CE seemed to stabilize for all storage conditions and cells.

Charge endpoints and voltage window.—Evaluating the endpoint slippage can help to analyze the capacity loss or to distinguish between side reactions. 32,52,69 In this study, the charge endpoint analysis tracks the charge delithiated from the cathode. The charge endpoints are normalized to the first charge with C/20 during formation. Figure 8a schematically shows the charge endpoints during formation for cells with and without anode overhang. The cells with an anode overhang exhibit increased charge endpoints for the second and third cycles compared to the 0% overhang cell. The same trend is observable for all cells in the first three cycles of Fig. 8b, where the charge endpoints for all six 30%, all six 8%, and the two 0% overhang cells at SOC50 are shown. The fourth cycle is during the cycle aging, in which the low CE was measured, as shown in Fig. 7. The charge endpoint of the fourth cycle shows only a slight increase for the cells with overhang and a slight decrease for the 0% overhang cells. The charge endpoint slippage tracks the maximum amount of lithium deintercalated from the NMC622 cathode.<sup>69</sup> The anode overhang seems to affect the delithiation state of the cathode. After the first three cycles, the charge endpoints remain almost constant, suggesting that the amount of delithiation is mostly affected during formation or early SEI growth.

Weng et al. reported a difference in loss of lithium inventory due to their two formation protocols. <sup>25</sup> In addition, their stacked pouch cells had large overhang areas of more than 20% due to double-side coated anode areas without a counter electrode. <sup>25</sup> Previous works show that anode overhang equalization leads to lithium moving into the overhang areas, comparable to loss of lithium inventory. <sup>7,13</sup> The amount of lithium moving into the anode overhang depends on the potential gradient between active and inactive anode areas. The potential gradient is ultimately given and impacted by the formation protocol. Consequently, the lithium consumption by the anode overhang can affect the amount of charge delithiated from the cathode, as shown in Fig. 8c. Further, Weng et al. commented in their supplemental that increased lithium consumption during formation might shift the voltage window of the positive electrode to

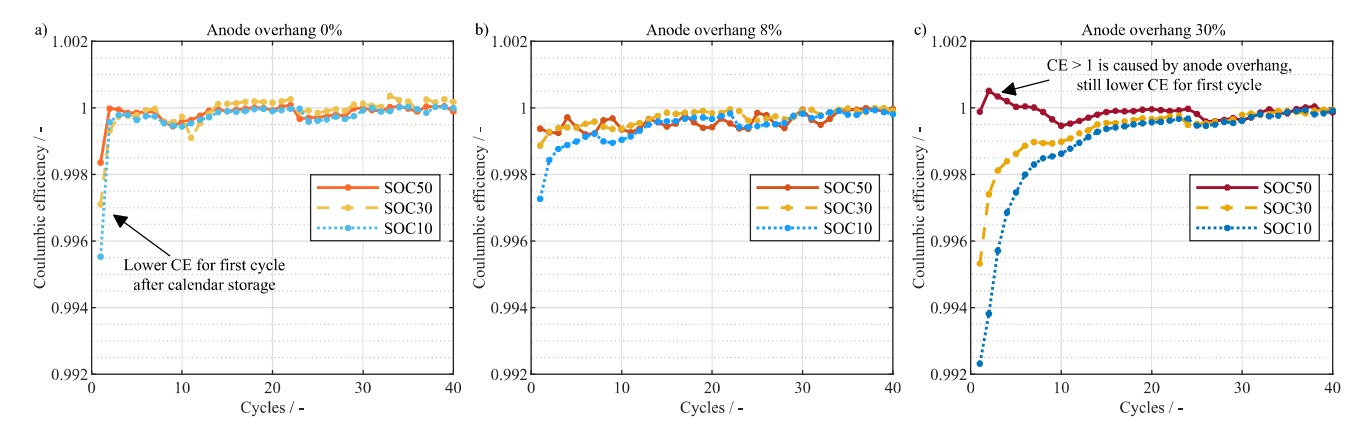
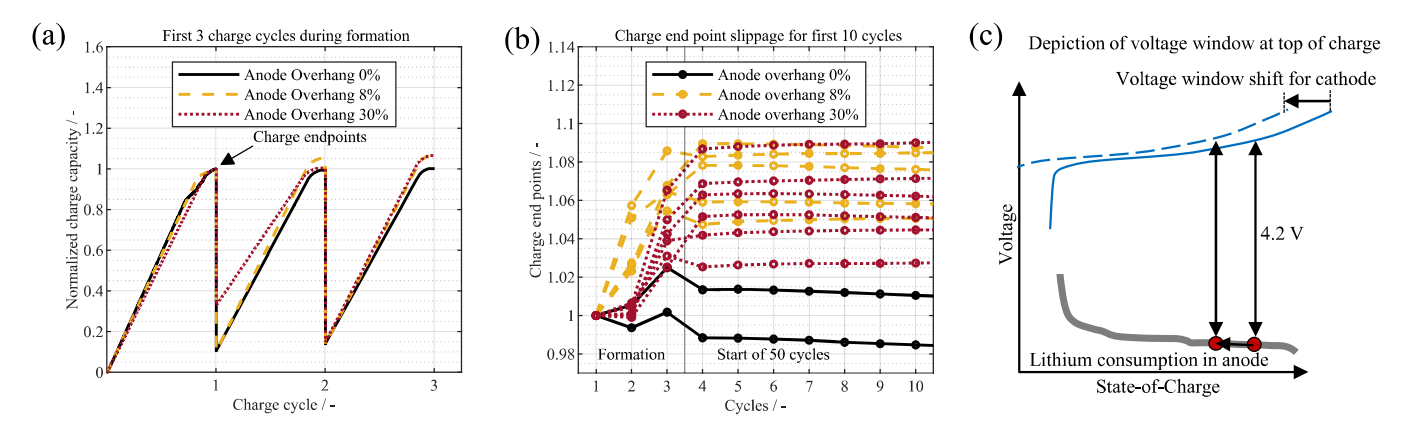


Figure 7. Coulombic efficiency of one cell at each SOC for (a) 0% overhang cells, (b) 8% overhang cells, and (c) 30% overhang cells. The first cycles after formation and calendar storage of 20 weeks show a lower CE, which indicates late SEI growth.



**Figure 8.** (a) Exemplary normalized capacity to evaluate the charge endpoints during formation. (b) Charge endpoint analysis for cells with and without anode overhang during formation and cycling. Cells with anode overhang show higher delithiation of the cathode, presumably due to increased lithium consumption by the overhang. (c) Schematic of the lithium consumption in the anode shifting the voltage window of the cathode to higher potentials at the top of charge.

higher potentials at the top of charge. The notion of irreversible lithium loss at the anode shifting the voltage window of the cathode to higher potentials has also been presented by Krueger et al. and Dose et al. Therefore, it is only plausible that the lithium movement into the anode overhang would similarly cause a shift in the voltage window of the positive electrode, as is illustrated in Fig. 8c. This mechanism might explain the reported positive impact of fast formation at higher cell voltages, 24.25 where lithium consumption during formation is increased by lithium movement into the anode overhang. It should be noted that the discharge phase of the 30% overhang cells ended earlier, which can also be seen in Fig. 8a. This small difference in the formation protocol could have reduced the charge endpoint slippage for the 30% overhang cells, which otherwise would be expected to be similar to or higher than the charge endpoint slippage of the 8% overhang cells in Fig. 8b.

Capacity evaluation.—Figure 9a shows the specific discharge capacity of the 30% overhang cells at the initial condition and after aging. All cells experienced the same formation protocol, and the initial capacity was measured before the calendar storage. Still, the initial capacity shows a spread over the six lab-made cells. This spread could not be fully explained, but a small inhomogeneity due to the electrode sheet coating, sheet cutting, or stack positioning could have caused it. After calendar storage and cycle aging, the aged capacity of the cells is more stable and close to a specific capacity of 140 mAh g<sup>-1</sup>. From the small sample size, aging data should not be overanalyzed, but the overall performance of the cells

does not seem to be reduced by the storage at SOC10. In fact, the opposite trend is shown by the two cells stored at SOC10 for 20 weeks, where the capacity is slightly higher than the storage at SOC30 and SOC50. The reduced aging at lower SOCs is in line with the calendar aging data reported in the literature. 27,72-74 evaluating the capacity retention of cells, the anode overhang equalization can cause significant capacity losses or recovery.<sup>4</sup> The relative behavior of capacity retention is often neglected and might not be representative of cell performance or quality. The capacity retention during 50 cycles at a constant current of C/3 between 3.0 V and 4.2 V for the 30% overhang cells is shown in Fig. 9b. Here, the relative data of the capacity retention might give the wrong impression that the cells stored at SOC10 had a worse cell performance because these cells showed a higher capacity loss during cycling. However, as shown in Fig. 9a, this is not the case. The capacity retention of the 0% and the 8% overhang cells is shown in supplemental S4. Figure 9c shows the specific discharge capacities of the two 0% overhang cells, which were stored at SOC50, all six 8%, and all six 30% overhang cells. The initial and aged cells with the larger anode overhang sizes showed an overall reduced capacity due to lithium moving into the anode overhang, which is the same trend previously reported by Son et al. 18 and Dagger et al. 19 This overall trend should not be mixed up with capacity loss due to calendar or cycle aging.

In summary, the impact of the anode overhang on capacity retention and capacity loss should be carefully considered when evaluating cell performance after formation as well as in general.

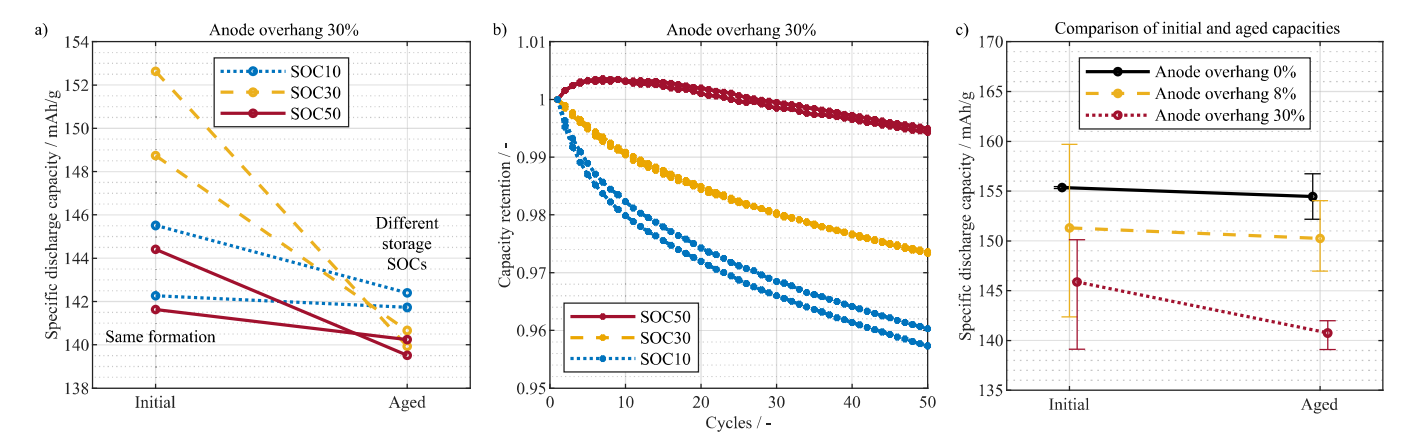


**Figure 9.** (a) Initial specific discharge capacity of the 30% overhang cells, where all cells experienced the same protocol, and the aged capacity, where the cells were stored at different SOCs. While the initial capacity shows a high spread, the aged capacity stabilizes at a specific capacity of approximately 140 mAh g<sup>-1</sup>. (b) Capacity retention during 50 cycles at a constant current of C/3 between 3.0 V and 4.2 V for 30% overhang cells. The relative data of capacity retention might give the wrong impression that the cells stored at SOC10 experienced higher capacity loss. (c) Initial and aged specific discharge capacities of the different anode overhang sizes show a trend of lower capacities for larger overhang areas.

#### **Conclusions**

Single-layer pouch cells with 0%, 8%, and 30% anode overhang were built, and the same formation protocol was applied to all cells. Then, the cells were stored at SOC10, SOC30, and SOC50, respectively. The voltage and the self-discharge current were measured over the first 100 h with the voltage decay method. Afterward, calendar storage at the same SOCs with a weekly voltage measurement was applied for 20 weeks to determine the long-term self-discharge current of the cells. After storage, all cells were cycled 50 times with a constant current of C/3, followed by a slow C/30 charge and discharge for ICA and DVA evaluation. Finally, the cell's aged capacity was determined similarly to the formation step. The main findings are summarized in the following:

- The self-discharge current at SOC10 showed less transient behavior compared to SOC30 and SOC50. At SOC30, the anode overhang leads to the measurement of increased selfdischarge current. At SOC50, the SEI growth starts to dominate the self-discharge rate. These findings suggest that self-discharge measurements in cells featuring graphite anodes may exhibit greater sensitivity to soft shorts or cell defects at lower SOCs due to less transient effects.
- All cells showed a lower coulombic efficiency for the first full cycle after a 20-week calendar storage. The lower CE correlated to the SOC during storage, but CE stabilized in subsequent cycles at all storage conditions. The results indicate that the SEI grows further at higher cell voltages or rather at low graphite anode potentials. The specific discharge capacity of the cells was also not impacted by the calendar storage at SOC10, SOC30, and SOC50.
- The cells with anode overhang showed a higher charge endpoint slippage during formation cycles, which suggests a higher delithiation of the NMC622 cathode. This could affect the amount of available lithium inventory in the full cell and shift the voltage window of the positive electrode to higher potentials at the top of charge. Such a shift in the voltage window might impact the cell performance.

Determining whether the interplay of formation protocol and lithium movement into the anode overhang affects the cell performance requires further investigation. Analyzing the cell resistance after formation could be a suitable method for helping to identify this relation. Weng et al. proposed a cell resistance measurement at low SOC as an early-life diagnostic for analyzing formation protocols.<sup>25</sup> This resistance measurement could also be combined with the self-discharge measurement at low SOC to optimize further and fasten characterization methods for LIB manufacturing. In this context, the effect of late SEI growth due to storage at low SOC on the cell performance was negligible for lab scale cells in this study. Still, the applicability and influence of fast self-discharge measurements at low SOC should also be investigated at pilot and industrial scale.

#### Acknowledgments

This work is financially supported by the German Federal Ministry of Education and Research (grant number 03XP0296D) and by the Technical University of Munich (TUM). The responsibility for this publication lies with the authors.

#### **ORCID**

Thomas Roth https://orcid.org/0000-0001-5543-2992 Luiza Streck https://orcid.org/0000-0001-5905-3308 Nedim Mujanovic https://orcid.org/0009-0008-8979-2847 Martin Winter https://orcid.org/0000-0003-4176-5811 Philip Niehoff https://orcid.org/0000-0001-8892-8978 Andreas Jossen https://orcid.org/0000-0003-0964-1405

#### References

- 1. A. Kwade, W. Haselrieder, R. Leithoff, A. Modlinger, F. Dietrich, and K. Droeder, 'Current status and challenges for automotive battery production technologies.' Nat. Energy, 3, 290 (2018).
- H.-H. Lee, Y.-Y. Wang, C.-C. Wan, M.-H. Yang, H.-C. Wu, and D.-T. Shieh, "A fast formation process for lithium batteries." J. Power Sources, 134, 118 (2004).
- 3. G. Bridgewater, M. J. Capener, J. Brandon, M. J. Lain, M. Copley, and E. Kendrick, "A comparison of lithium-ion cell performance across three different cell formats." Batteries, 7, 38 (2021).
- 4. B. Gyenes, D. A. Stevens, V. L. Chevrier, and J. R. Dahn, "Understanding anomalous behavior in coulombic efficiency measurements on li-ion batteries. Electrochem. Soc., 162, A278 (2015).
- J. Wilhelm, S. Seidlmayer, P. Keil, J. Schuster, A. Kriele, R. Gilles, and A. Jossen, 'Cycling capacity recovery effect: a coulombic efficiency and post-mortem study.' J. Power Sources, 365, 327 (2017).
- M. Lewerenz, G. Fuchs, L. Becker, and D. U. Sauer, "Irreversible calendar aging and quantification of the reversible capacity loss caused by anode overhang. J. Energy Storage, 18, 149 (2018).
- 7. F. Hildenbrand, D. Ditscheid, E. Barbers, and D. U. Sauer, "Influence of the anode overhang on the open-circuit voltage and the ageing of lithium-ion batteries-A
- model based study." *Appl. Energy*, **332**, 120395 (2023).

  8. J. P. Fath, L. Alsheimer, M. Storch, J. Stadler, J. Bandlow, S. Hahn, R. Riedel, and T. Wetzel, "The influence of the anode overhang effect on the capacity of lithium-
- ion cells—a 0D-modeling approach." *J. Energy Storage*, **29**, 101344 (2020). R. Burrell, A. Zulke, P. Keil, and H. Hoster, "Communication—identifying and managing reversible capacity losses that falsify cycle ageing tests of lithium-ion J. Electrochem. Soc., 167, 130544 (2020).
- 10. T. Hüfner, M. Oldenburger, B. Bedürftig, and A. Gruhle, "Lithium flow between active area and overhang of graphite anodes as a function of temperature and overhang geometry." *J. Energy Storage*, **24**, 100790 (2019).

  I. Zilberman, J. Sturm, and A. Jossen, "Reversible self-discharge and calendar aging
- of 18650 nickel-rich, silicon-graphite lithium-ion cells." J. Power Sources, 425, 217
- 12. M. Theiler, C. Endisch, and M. Lewerenz, "Float current analysis for fast calendar aging assessment of 18650 Li(NiCoAl)O<sub>2</sub>/graphite cells." Batteries, 7, 22 (2021).
- 13. T. Roth, L. Streck, A. Graule, P. Niehoff, and A. Jossen, "Relaxation effects in selfdischarge measurements of lithium-ion batteries." J. Electrochem. Soc., 170, 020502 (2023).
- 14. M. Azzam, M. Ehrensberger, R. Scheuer, C. Endisch, and M. Lewerenz, "Longterm self-discharge measurements and modelling for various cell types and cell potentials." *Energies*, **16**, 3889 (2023).
- M. Lewerenz, J. Münnix, J. Schmalstieg, S. Käbitz, M. Knips, and D. U. Sauer, Systematic aging of commercial lifepo 4 Igraphite cylindrical cells including a theory explaining rise of capacity during aging." J. Power Sources, 345, 254 (2017).
- M. Tang, P. Albertus, and J. Newman, "Two-dimensional modeling of lithium deposition during cell charging." *J. Electrochem. Soc.*, 156, A390 (2009).
   C. Hogrefe, T. Waldmann, M. Hölzle, and M. Wohlfahrt-Mehrens, "Direct
- observation of internal short circuits by lithium dendrites in cross-sectional lithium-ion in situ full cells." *J. Power Sources*, **556**, 232391 (2023).
- 18. B. Son, M.-H. Ryou, J. Choi, S.-H. Kim, J. M. Ko, and Y. M. Lee, "Effect of cathode/anode area ratio on electrochemical performance of lithium-ion batteries." Power Sources, 243, 641 (2013).
- 19. T. Dagger, J. Kasnatscheew, B. Vortmann-Westhoven, T. Schwieters, S. Nowak, M. Winter, and F. M. Schappacher, "Performance tuning of lithium ion battery cells with area-oversized graphite based negative electrodes." J. Power Sources, 396, 519
- 20. F. Grimsmann, T. Gerbert, F. Brauchle, A. Gruhle, J. Parisi, and M. Knipper, "Hysteresis and current dependence of the graphite anode color in a lithium-ion cell and analysis of lithium plating at the cell edge." *J. Energy Storage*, **15**, 17 (2018). Y. Lee, B. Son, J. Choi, J. H. Kim, M.-H. Ryou, and Y. M. Lee, "Effect of back-
- side-coated electrodes on electrochemical performances of lithium-ion batteries." J. Power Sources, 275, 712 (2015).
- S. J. An, J. Li, Z. Du, C. Daniel, and D. L. Wood, "Fast formation cycling for lithium ion batteries." J. Power Sources, 342, 846 (2017).
- C. Mao, S. J. An, H. M. Meyer, J. Li, M. Wood, R. E. Ruther, and D. L. Wood, "Balancing formation time and electrochemical performance of high energy lithium-ion batteries." J. Power Sources, 402, 107 (2018).
- V. Müller, R. Kaiser, S. Poller, and D. Sauerteig, "Importance of the constant voltage charging step during lithium-ion cell formation." J. Energy Storage, 15, 256 (2018).
- 25. A. Weng, P. Mohtat, P. M. Attia, V. Sulzer, S. Lee, G. Less, and A. Stefanopoulou, Predicting the impact of formation protocols on battery lifetime immediately after manufacturing." Joule, 5, 2971 (2021).
- R. Drees, F. Lienesch, and M. Kurrat, "Fast charging formation of lithium-ion batteries based on real-time negative electrode voltage control." Energy Technol., 11, 479 (2023).
- P. Keil, S. F. Schuster, J. Wilhelm, J. Travi, A. Hauser, R. C. Karl, and A. Jossen, "Calendar aging of lithium-ion batteries." *J. Electrochem. Soc.*, 163, A1872 (2016).
   C. Rahe, S. T. Kelly, M. N. Rad, D. U. Sauer, J. Mayer, and E. Figgemeier,
- 'Nanoscale X-ray imaging of ageing in automotive lithium ion battery cells.' I. Power Sources, 433, 126631 (2019).
- 29. D. L. Wood, J. Li, and S. J. An, "Formation challenges of lithium-ion battery manufacturing." Joule, 3, 2884 (2019).

- 30. Y. Liu, R. Zhang, J. Wang, and Y. Wang, "Current and future lithium-ion battery manufacturing." iScience, 24, 102332 (2021).
- M. Broussely, S. Herreyre, P. Biensan, P. Kasztejna, K. Nechev, and R. J. Staniewicz, "Aging mechanism in Li ion cells and calendar life predictions." *J. Power Sources*, **97–98**, 13 (2001).
- 32. A. J. Smith, J. C. Burns, X. Zhao, D. Xiong, and J. R. Dahn, "A high precision coulometry study of the sei growth in li/graphite cells." J. Electrochem. Soc., 158,
- 33. M. Tang, S. Lu, and J. Newman, "Experimental and theoretical investigation of solid-electrolyte-interphase formation mechanisms Electrochem. Soc., 159, A1775 (2012).
- 34. R. Mogensen, D. Brandell, and R. Younesi, "Solubility of the solid electrolyte interphase (SEI) in sodium ion batteries." ACS Energy Lett., 1, 1173 (2016).
- E. Peled and S. Menkin, "Review—sei: past, present and future." J. Electrochem. Soc., 164, A1703 (2017).
- 36. P. M. Attia, W. C. Chueh, and S. J. Harris, "Revisiting the  $t^{0.5}$  dependence of sei growth." J. Electrochem. Soc., 167, 090535 (2020).
- 37. E. Markevich, M. D. Levi, and D. Aurbach, "New insight into studies of the cycling performance of li-graphite electrodes." J. Power Sources, 152, A778 (2005).
- 38. M. Lewerenz and D. U. Sauer, "Evaluation of cyclic aging tests of prismatic automotive LiNiMnCoO2-Graphite cells considering influence of homogeneity and anode overhang." *J. Energy Storage*, **18**, 421 (2018).

  A. Tornheim and D. C. O'Hanlon, "What do coulombic efficiency and capacity
- retention truly measure? a deep dive into cyclable lithium inventory, limitation type, and redox side reactions." J. Electrochem. Soc., 167, 110520 (2020).
- 40. O. C. Harris, S. E. Lee, C. Lees, and M. Tang, "Review: mechanisms and consequences of chemical cross-talk in advanced li-ion batteries." J. Phys. Energy, 032002 (2020).
- 41. S. Buechele, E. Logan, T. Boulanger, S. Azam, A. Eldesoky, W. Song, M. B. Johnson, and M. Metzger, "Reversible self-discharge of LFP/Graphite and NMC811/graphite cells originating from redox shuttle generation." J. Electrochem. Soc., 170, 010518 (2023).
- 42. X. Zhang, E. Sahraei, and K. Wang, "Li-ion battery separators, mechanical integrity and failure mechanisms leading to soft and hard internal shorts." Sci. Rep., 6, 32578 (2016).
- 43. L. Huang et al., "A review of the internal short circuit mechanism in lithium-ion batteries: Inducement, detection and prevention." Int. J. Energy Res., 45, 15797
- 44. D. J. Xiong, R. Petibon, M. Nie, L. Ma, J. Xia, and J. R. Dahn, "Interactions between positive and negative electrodes in li-ion cells operated at high temperature and high voltage." J. Electrochem. Soc., 163, A546 (2016).
- N. R. Vadivel, S. Ha, M. He, D. Dees, S. Trask, B. Polzin, and K. G. Gallagher, "On Leakage current measured at high cell voltages in lithium-ion batteries. Electrochem. Soc., 164, A508 (2017).
- 46. S. L. Glazier, S. A. Odom, A. P. Kaur, and J. R. Dahn, "Determining parasitic reaction enthalpies in lithium-ion cells using isothermal microcalorimetry.' J. Electrochem. Soc., 165, A3449 (2018).
- 47. E. R. Logan, H. Hebecker, X. Ma, J. Quinn, Y. HyeJeong, S. Kumakura, J. Paulsen, and J. R. Dahn, "A comparison of the performance of different morphologies of LiNi<sub>0.8</sub>Mn<sub>0.1</sub>Co<sub>0.1</sub>O<sub>2</sub> Using isothermal microcalorimetry, ultra-high precision coulometry, and long-term cycling." J. Electrochem. Soc., 167, 060530 (2020).
- 48. T. Boulanger, A. Eldesoky, S. Buechele, T. Taskovic, S. Azam, C. Aiken, E. Logan, and M. Metzger, "Investigation of redox shuttle generation in LFP/Graphite and NMC811/graphite cells." *J. Electrochem. Soc.*, **169**, 040518 (2022).
- S. Buechele et al., "Identification of redox shuttle generated in LFP/Graphite and NMC811/Graphite Cells." *J. Electrochem. Soc.*, **170**, 010511 (2023).
- 50. J. B. Goodenough and Y. Kim, "Challenges for rechargeable li batteries." Chem. Mater., 22, 587 (2010).
- 51. R. Jung, M. Metzger, F. Maglia, C. Stinner, and H. A. Gasteiger, "Oxygen release and its effect on the cycling stability of LiNixMnyCozO2 (NMC) cathode materials for li-ion batteries." J. Electrochem. Soc., 164, A1361 (2017).

- 52. P. Keil and A. Jossen, "Calendar aging of NCA lithium-ion batteries investigated by differential voltage analysis and coulomb tracking." J. Electrochem. Soc., 164, A6066 (2017).
- 53. L. Streck, T. Roth, P. Keil, B. Strehle, S. Ludmann, and A. Jossen, "A comparison of voltage hold and voltage decay methods for side reactions characterization. Electrochem. Soc., 170, 040520 (2023).
- 54. S. M. P. Jagfeld, K. P. Birke, A. Fill, and P. Keil, "How cell design affects the aging behavior: comparing electrode-individual aging processes of high-energy and highpower lithium-ion batteries using high precision coulometry." *Batteries*, **9**, 232 (2023).
- B. Horstmann et al., "Strategies towards enabling lithium metal in batteries: interphases and electrodes." *Energy Environ. Sci.*, **14**, 5289 (2021).
  56. Z. Chen, R. Amine, Z.-F. Ma, and K. Amine, "Interfacial reactions in lithium
- batteries." J. Phys. D, 50, 303001 (2017).
- 57. F. German, A. Hintennach, A. LaCroix, D. Thiemig, S. Oswald, F. Scheiba, M. J. Hoffmann, and H. Ehrenberg, "Influence of temperature and upper cut-off voltage on the formation of lithium-ion cells." *J. Power Sources*, **264**, 100 (2014).
- K. Kleiner, P. Jakes, S. Scharner, V. Liebau, and H. Ehrenberg, "Changes of the balancing between anode and cathode due to fatigue in commercial lithium-ion cells." J. Power Sources, 317, 25 (2016).
- J. Kasnatscheew, T. Placke, B. Streipert, S. Rothermel, R. Wagner, P. Meister, I. C. Laskovic, and M. Winter, "A tutorial into practical capacity and mass balancing of lithium ion batteries." *J. Electrochem. Soc.*, 164, A2479 (2017).
  60. C.-S. Kim, K. M. Jeong, K. Kim, and C.-W. Yi, "Effects of capacity ratios between
- anode and cathode on electrochemical properties for lithium polymer batteries.' Electrochim, Acta, 155, 431 (2015).
- 61. F. Schomburg, R. Drees, M. Kurrat, M. A. Danzer, and F. Röder, "Characterization of the solid-electrolyte interphase growth during cell formation based on differential voltage analysis." *Energy Technol.*, **223**, 2200688 (2022).
- F. M. Kindermann, A. Noel, S. V. Erhard, and A. Jossen, "Long-term equalization effects in Li-ion batteries due to local state of charge inhomogeneities and their impact on impedance measurements." Electrochim. Acta, 185, 107 (2015).
- A. H. Zimmerman, "Self-discharge losses in lithium-ion cells." IEEE Aerosp. Electron. Syst. Mag., 19, 19 (2004).
- 64. P. Münster, M. Winter, and P. Niehoff, "A method to determine fast charging procedures by operando overvoltage analysis." J. Electrochem. Soc., 169, 070525 (2022).
- 65. M. Lewerenz, P. Dechent, and D. U. Sauer, "Investigation of capacity recovery during rest period at different states-of-charge after cycle life test for prismatic Li(Ni<sub>1/3</sub>Mn<sub>1/3</sub>Co<sub>1/3</sub>)O<sub>2</sub>-graphite cells." *J. Energy Storage*, **21**, 680 (2019).
- L. Köbbing, A. Latz, and B. Horstmann, J. Power Sources, 561, 232651 (2023).
- T. Ma et al., "Revisiting the corrosion of the aluminum current collector in lithium-
- ion batteries." *J. Phys. Chem. Lett.*, **8**, 1072 (2017).
  68. H. Gao et al., "Parasitic reactions in nanosized silicon anodes for lithium-ion batteries." Nano Lett., 17, 1512 (2017).
- R. D. Deshpande, P. Ridgway, Y. Fu, W. Zhang, J. Cai, and V. Battaglia, "The limited effect of VC in graphite/NMC Cells." J. Electrochem. Soc., 162, A330 (2015).
- S. Krueger, R. Kloepsch, J. Li, S. Nowak, S. Passerini, and M. Winter, "How do reactions at the anode/electrolyte interface determine the cathode performance in lithium-ion batteries?" J. Electrochem. Soc., 160, A542 (2013).
- W. M. Dose, C. Xu, C. P. Grey, and M. F. L. D. Volder, "Effect of anode slippage on cathode cutoff potential and degradation mechanisms in ni-rich li-ion batteries. Cell Rep. Phys. Sci., 1, 100253 (2020).
- A. Zülke, Y. Li, P. Keil, R. Burrell, S. Belaisch, M. Nagarathinam, M. P. Mercer, and H. E. Hoster, "High-energy nickel-cobalt-aluminium oxide (NCA) cells on idle: anode- versus cathode-driven side reactions." *Batter. Supercaps*, **4**, 849 (2021).
- 73. M. Ecker, N. Nieto, S. Käbitz, J. Schmalstieg, H. Blanke, A. Warnecke, and D. U. Sauer, "Calendar and cycle life study of Li(NiMnCo)O2-based 18650 lithiumion batteries." J. Power Sources, 248, 839 (2014).
- 74. K. Smith, P. Gasper, A. M. Colclasure, Y. Shimonishi, and S. Yoshida, "Lithiumion battery life model with electrode cracking and early-life break-in processes." J. Electrochem. Soc., 168, 100530 (2021).